
Project Title:

**Innovative compact HYbrid electrical/thermal storage systems for low energy BUILDings**

Project Acronym:

**HYBUILD**

**Grant Agreement Nº: 768824**

**Collaborative Project**

# Deliverable Report

Deliverable number:

## D2.3

Deliverable title:

# DC driven compression heat pump tests successful

| | |
|---|---|
| **Related task:** | 2.3 |
| **Lead beneficiary:** | CNR |
| **Authors and institutions:** | CSEM - Nelson Koch, Pierre-Jean Alet<br>AIT – Klemens Marx, Tilman Barz, Johann Emhofer<br>OCHS - Michael Wiesflecker<br>NTUA - Sotirios Karellas, Stratis Varvagiannis<br>DAIK - Nikolaos Barmparitsas<br>CNR - Andrea Frazzica, Valeria Palomba |
| **Due date:** | M24 - 30th of September 2019 |

*This project has received funding from the* European Union's Horizon 2020 research and innovation programme *under grant agreement No 768824.*

| DISSEMINATION LEVEL | | |
|---|---|---|
| PU | Public, fully open, e.g. web | X |
| CO | Confidential, restricted under conditions set out in Model Grant Agreement | |
| CI | Classified, information as referred to in Commission Decision 2001/844/EC. | |

| DOCUMENT STATUS HISTORY | | |
|---|---|---|
| Date | Description | Partner |
| 2019/08/09 | Version 1 | CSEM |
| 2019/08/26 | Version 2 | AIT |
| 2019/08/27 | Revised version | CNR |
| 2019/09/02 | First complete version | CNR |
| 2019/09/03 | Finalized revision | CNR |
| 2019/09/20 | Internal quality review completed | UDL, R2M, COMSA |

# Table of contents

## Publishable executive summary

HYBUILD is an EU Horizon 2020 - funded project, led by COMSA Corporación, which will develop two innovative compact hybrid electrical/thermal storage systems for stand-alone and district connected buildings.

The present deliverable presents the activities done within T2.3 on the development of DC-driven compression heat pumps for both the HYBUILD Continental system and the HYBUILD Mediterranean system. The heat pumps integrate the RPW-HEX (latent storage) described in D2.2 and have been modified to allow the operation in DC.

The integration of the heat pumps in a DC microgrid requires suitable converters, which were selected according to technical and economic constraints given by CSEM. In particular, recommendations were made for the AC/DC grid converters, the DC/DC converters for the integration with the electrical storage described in D2.4, and the DC/DC converter for PV systems that might be available. In addition, a user interface was realised, to simplify monitoring and supervision during the installation in HYBUILD demonstration sites.

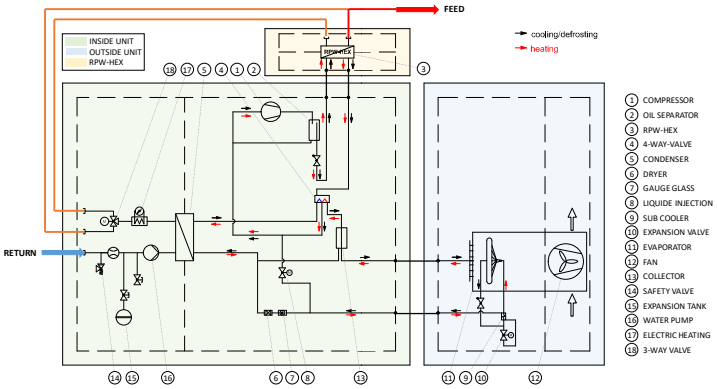


The compression heat pump to be used in the Continental system is equipped with a frequency converter. On the other hand, the Mediterranean heat pump is using a fixed speed compressor, so a separate frequency drive for the compressor has been selected and installed. On the Continental system, the heat pump developed by AIT and OCHS with the integrated RPW-HEX developed by AKG was tested in a controlled laboratory environment at AIT. The tests showed the system can handle DC supply voltages in the design range without any interruption in the operation and that the efficiency decreases with increasing DC supply voltage

In the case of the Mediterranean heat pump, developed by DAIK and NTUA, selected results from the preliminary tests of the heat pump before and after interventions regarding the installation of the electrical components for DC operation and of the RPW-HEX are presented. The results allowed the identification of the most suitable AC/DC converter for the compressor and the verification that the changes due to the installation of the electrical components and the RPW-HEX did not affect the operation of the compressor.

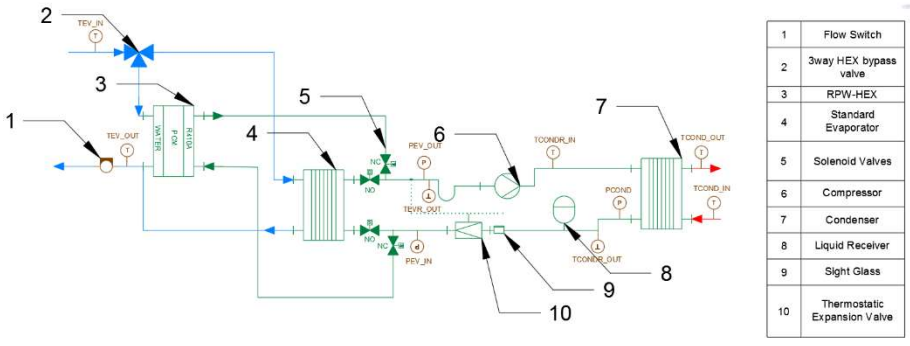


Besides, monitoring protocols for the instantaneous and seasonal performance indicators of both the heat pumps, based on real time data available from the installed sensors, were defined. Even though measuring the instantaneous COP and EER values for the Continental and the Mediterranean heat pumps respectively can be achieved through assumptions (and

provided that the state of the refrigerant at the outlet of the condenser is not in the two-phase region for the continental design), using a Seasonal Performance Factor based on the measured values on the water side for both the system can directly lead to more reliable results, provided that this Factor refers to a long enough time period.

## Acronyms and Abbreviations

| **Nomenclature** | |
|---|---|
| E | Energy, J |
| i | Current, A |
| h | Enthalpy, J |
| $\dot{m}$ | Mass flow rate, kg/s |
| p | Pressure, bar |
| P | Power, W |
| $\dot{Q}$ | Thermal power, W |
| t | Time, s |
| u | Voltage, V |
| Θ | Temperature, °C |
| **Subscripts** | |
| cond | Condenser |
| el | electric |
| evap | Evaporator |
| loss | Thermal Losses |
| PCM | Phase Change Material |
| r | Refrigerant |
| th | thermal |
| W | water |
| **Abbreviations** | |
| BEMS | Building Energy Management System |
| BMU | Building Maintenance Unit |
| CPF | Cycle Performance Factor |
| COP | Coefficient of performance |
| EER | Energy Efficiency Ratio |
| FTI | Flow Transducer/Indicator |
| HEX | Heat Exchanger |
| HP | Heat Pump |
| PDTI | Differential Pressure Transducer/Indicator |
| PF | Performance Factor |
| PI | Pressure Indicator |
| PT | Pressure Transducer |
| PV | Photovoltaic |
| RPW | Refrigerant-PCM-Water |
| SPF | Seasonal Performance Factor |
| TI | Temperature Indicator |
| TT | Temperature Transducer |
| UI | User Interface |

# 1 Introduction

## 1.1 Aims and objectives

In the present deliverable, the development of DC bus architecture and its integration with the heat pumps under lab-controlled conditions is reported. The process of selection of converters, based on operating and economic constraints, is presented. A specific user interface, suitable for the control and supervision of the converters and data of the smart meters was developed as well. Subsequently, the installation and operation of the heat pumps equipped with a minimal DC bus was carried out in laboratory settings with hardware in the loop for both Mediterranean and Continental heat pumps, verifying the operation under transient controlled conditions. Furthermore, the feasibility of advanced process monitoring algorithms for online estimation of performance parameters, such as the coefficient of performance of the heat pumps and the actual thermal and electrical power was validated. Final outcome of the deliverable was the definition of the main DC-bus architecture and the verification of DC-driven operation of heat pumps, including the provision of key variables for the smart high-level control strategy.

## 1.2 Relations to other activities in the project

The activity presented in this report was carried out within task 2.3, with the aim of validating the efficiency of the DC interconnection approach in a lab environment, that was developed within task 3.2 and described in D3.2. The sub-systems developed will be integrated and the overall Mediterranean and Continental systems will be tested under controlled boundaries in WP3. The monitoring activity, through the definition of suitable algorithms, will allow the development of the control structure in WP4.

## 1.3 Report structure

The report is structured as follows:

- Section 2 presents the generic description of the DC-driven heat pumps for Mediterranean and Continental HYBUILD solutions;
- Section 3 presents the selection of DC converters and the development of a User Interface to facilitate control and supervision in demo sites.
- Section 4 presents the integration of the heat pump with the converters. In particular, section 4.2 describes the integration for the Continental solutions, section 4.3 the integration of the Mediterranean solution and section 4.4 the evaluation of online parameters for integration with the BEMS.

## 1.4 Contributions of partners

CSEM defined the selection of the DC microgrid inverters, DAIK and OCHS provided the heat pumps and AKG provided the RPW-HEX that were installed and tested in the labs of AIT and NTUA. CNR supervised the deliverable preparation.

# 2 Description of the heat pump technologies for heating and cooling

## 2.1 Heat pump for the Continental system

The heat pump for the Continental system is a water/air type heat pump : it includes an inside unit, an outside unit and the RPW-HEX. The units are pre-assembled and shall be connected by suitable pipes on-site. The process flow diagram of the compression heat pump setup in the Continental system is depicted in Figure 1.

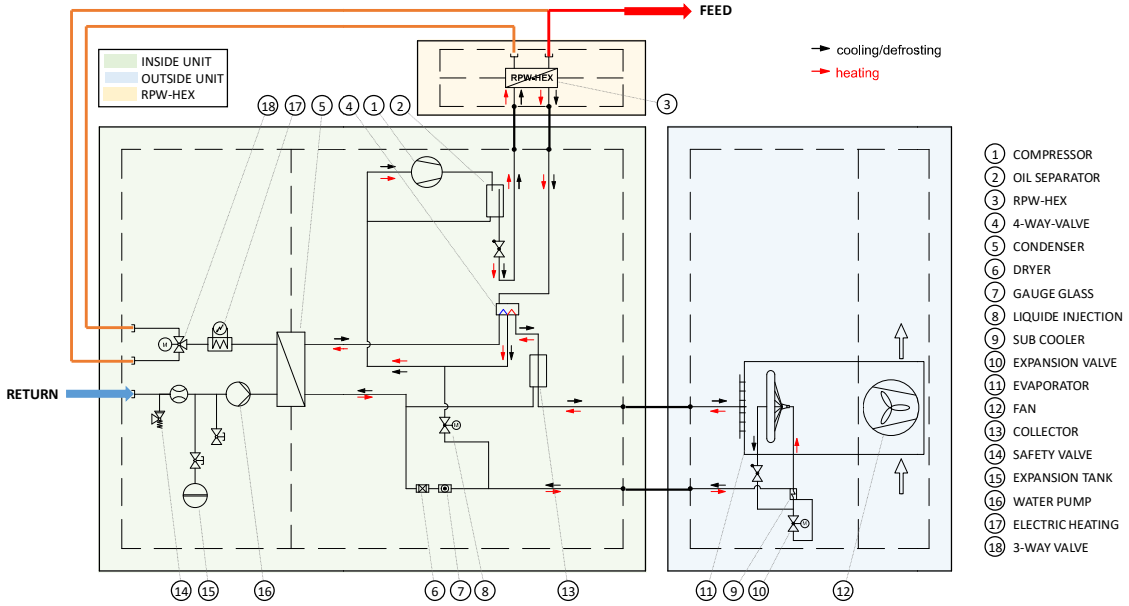


Figure 1 Process flow diagram of the compression heat pump setup in the continental system.

In the inside unit the compressor ① is placed which is driven by a variable speed drive and allows for AC and DC-supply as well (see section 4.1). After passing the oil separator ② the hot compressor exhaust passes the RPW-HEX ③ where heat is effectively recovered at high temperature. The 4-way valve ④ allows to reverse the flow of the refrigerant and facilitates either cooling or defrosting operation. In heating mode operation, the hot refrigerant is directed to the condenser ⑤ to heat the water or to the condenser in defrosting or cooling operation. After passing a filter dryer ⑥ and a gauge glass ⑦ the refrigerant is subcooled in the sub cooler ⑨, expanded in the expansion valve ⑩ before entering the evaporator ⑪. A fan ⑫ is used to increase the heat transfer performance of the evaporator where the fan speed is controlled depending on the operating conditions. A small refrigerant collector ⑬ is used to allow efficient operation over a wide operating range. The 4-way-valve closes the refrigerant cycle and directs the refrigerant to the compressor suction side. To limit the temperature of the compressor exit – a peculiarity of the R32 refrigerant – liquid refrigerant is injected into the compressor suction side using the liquid injection valve ⑧. In cooling or defrosting operation, the 4-way-valves will direct the hot refrigerant to the evaporator, where it condenses releasing heat. The cold refrigerant then passes the condenser where it evaporates absorbing low temperature heat for cooling. The operation modes of the 4-way valve are illustrated in Figure 2.

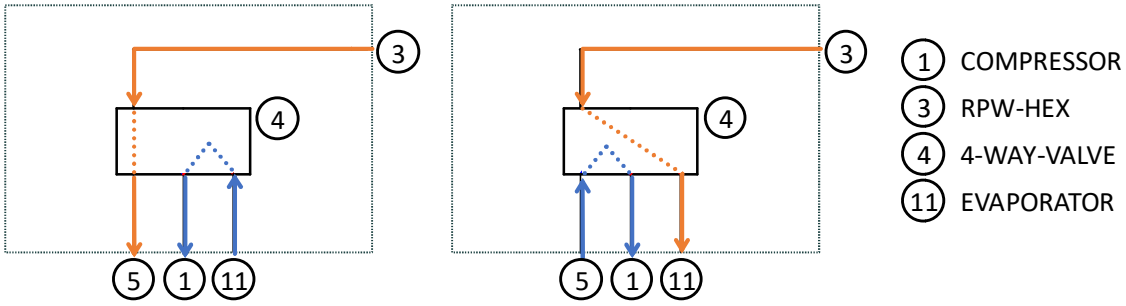


Figure 2 4-way valve operation. Left: Heating mode operation. Right: Defrosting or cooling mode operation.

In the water side a safety valve ⑭ is placed to avoid overpressure in the water circuit of the heat pump. To compensate for the density fluctuation the expansion tank ⑮ is placed. The water pump ⑯ compensates for the pressure drop of the condenser. After passing the condenser an electric heater ⑰ allows to cover the demand whenever the heat pump delivers insufficient thermal power. To control the feed water temperature the 3-way valve ⑱ is used allowing to direct the water from the condenser to the feed directly or the RPW-HEX.

## 2.2 Heat pump for the Mediterranean system

The Mediterranean heat pump unit is of the water/water type providing the option to connect the sorption chiller on top of its condenser. A schematic with the components and the installed sensors on the heat pump is depicted in Figure 3:

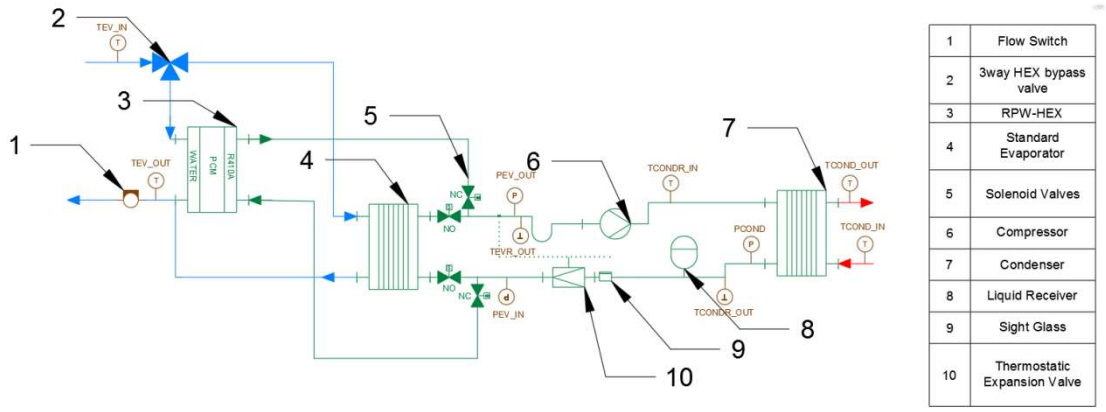


| | |
|---|---|
| 1 | Flow Switch |
| 2 | 3way HEX bypass valve |
| 3 | RPW-HEX |
| 4 | Standard Evaporator |
| 5 | Solenoid Valves |
| 6 | Compressor |
| 7 | Condenser |
| 8 | Liquid Receiver |
| 9 | Sight Glass |
| 10 | Thermostatic Expansion Valve |

Figure 3 Schematic diagram of the compression heat pump setup in lab for the Mediterranean concept (installed sensors marked in red)

The refrigerant circuit is typical of a conventional water chiller design, consisting of a hermetic scroll compressor (6), a Thermostatic Expansion Valve (10) and two plate heat exchangers, the evaporator (4) and the condenser (7). No 4way valve is installed and thus, if heating is needed, the hydraulic circuits of the evaporator and the condenser need to be swapped by means of 3-way valves. The state of the refrigerant flow after the condenser may be determined using the sight glass (9). The RPW-HEX (4) actually replaces the standard evaporator in cooling mode. In order to maintain the option to operate the heat pump with the standard evaporator (useful especially in heating mode), bypass loops have been implemented in both the refrigerant and the water circuits. In the water side, a 3way ball valve (2) connects either the standard evaporator or the RPW-HEX to the water supply pipeline. The motor of the valve was selected in order to allow fast switching between the two modes in order to prevent evaporator

freezing (running time of 45 sec for RPW-HEX and 24 sec for the standard evaporator), while its design permits the switching of the heat exchangers during operation without affecting the Flow Switch (1), which is installed on the outlet of both the heat exchangers. If the charging mode of the RPW-HEX is needed to be tested (thus no water flow is desired in the heat exchanger), the flow switch needs to be bypassed from the control unit of the heat pump. On the refrigerant side, four solenoid valves allow the immediate switching between the two heat exchangers. The solenoids connected to the standard evaporator ports are Normally Open (NO), while the ones connected to the RPW-HEX are Normally Closed (NC). Since the 3way valve on the water side is diverting the flow in the RPW-HEX only when it is electrically connected, the heat pump is reverted to the standard evaporator in case of automation system power loss. Lastly, since a large discrepancy among the refrigerant charge needed among the RPW-HEX and the standard evaporator was identified, the installation of a liquid receiver at the exit of the condenser is scheduled.

The retrofitted Mediterranean heat pump is being tested in the laboratory of NTUA, shown in Figure 4. The test rig has been upgraded since the M12 of the project and thus it was supposed that making a brief description of the performed changes from the initial setup described in D3.2[1] is important. In addition, the installed sensors on the hydraulic circuits are also critical for the implementation of the monitoring algorithms (see section 5.1.2):

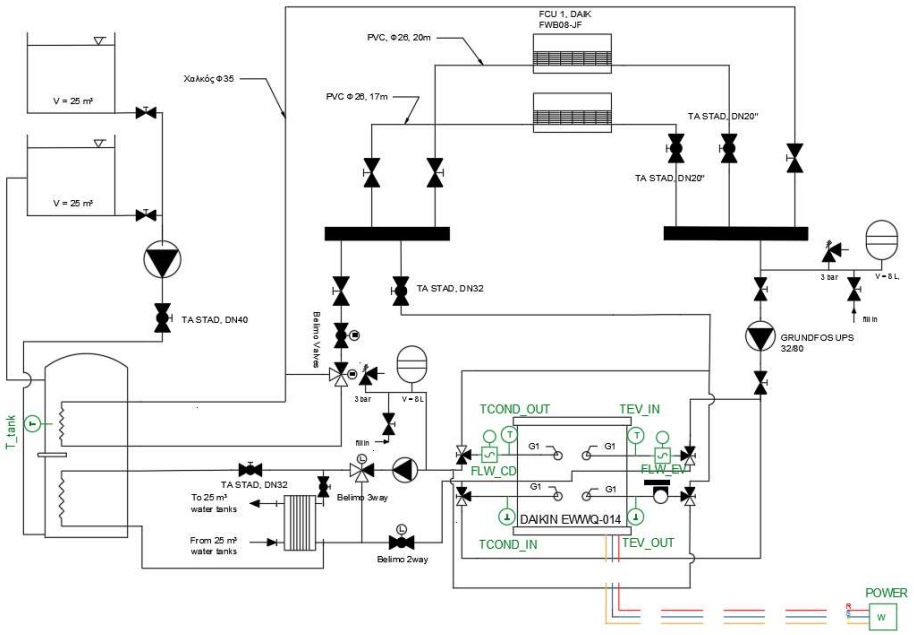


Figure 4 Schematic of NTUA's most recent test rig and sensors (marked green)

As for the previous version of the test rig, the heat of the condenser is rejected to two 25m³ open water tanks having water in almost ambient conditions via a small plate heat exchanger, while the useful cooling of the evaporator can be directed two Fan Coil Units, each with 7kW$_{th}$ rated power. The operation of the heat pump can be swapped from cooling to heating mode (and thus rejecting the condenser heat to the Fan Coil Units and absorbing the required heat by the evaporator from the water tanks) by means of four 3way ball valves. As described in D3.2, all the temperatures are measured by means of pT-100 RTD sensors, while the electrical variables are measured using a panel mounted electrical network analyzer. Two new ultrasonic flow sensors were installed in fixed positions in the evaporator and condenser circuits for better accuracy, avoiding the usage of portable measuring instruments. All the signals from the sensors installed in the heat pump setup and the test-rig are collected using Advantech's

[1] See Deliverable D3.2 – "Configuration of the hard- and software interfaces of the DCS finished"

ADAM modules and are logged in an industrial PC programmed with LabView. The same LabView application allows the control of the heat pump and the installed actuators through ADAM digital and analog I/O modules.

The most important modification of the old test rig is the addition of an 1m³ insulated water tank with two immersed heat exchangers, which are connected to both the evaporator and the condenser of the heat pump respectively, allowing the testing in various temperature conditions independently of heating demand of the room. Water from the water 25 m³ tanks is also flowing through the smaller tank in order to achieve heat balance. Besides, regulation of the inlet temperatures in the condenser and the evaporator is possible through mixing with the return stream using two 3way control valves. The water mass flow rate entering the heat exchangers of the heat pump can be controlled by means of two 2way control valves, allowing the testing under controllable ΔT (usually a ΔT of 5°C is desired during performance tests). The plate heat exchanger of the initial test rig can also be used in order to reject part of the condenser heat and permit to control even better the condenser temperature conditions.

The real test rig with is shown in the following pictures:

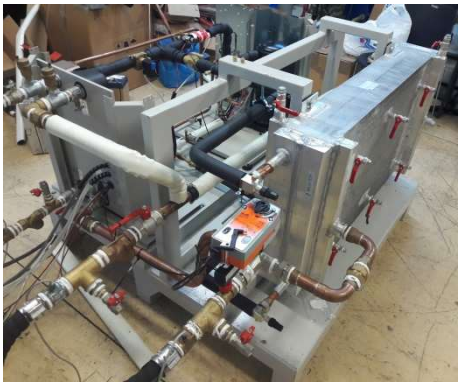

Figure 5 The retrofitted heat pump along with the RPW-HEX

Figu the


Figure 7 Press he refrigerant circu bar)

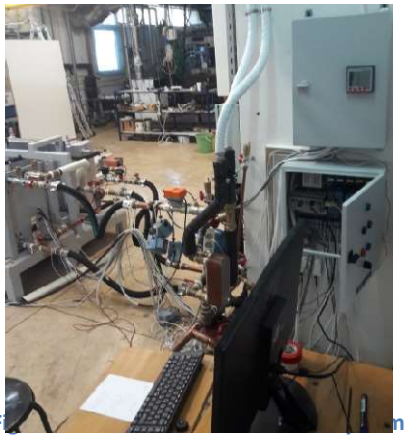

F n panels and actuators under installation

# 3 Selection of DC microgrid converters

In this section the method applied for the selection of the DC microgrid converters is presented. First, the overall electrical characteristics of the DC microgrid are presented. Then, the system constraints will be defined. Finally based on these constraints, the selected devices will be presented.

## 3.1 Electrical characteristics of the DC bus

The topology of the electrical system is illustrated in Figure 9.

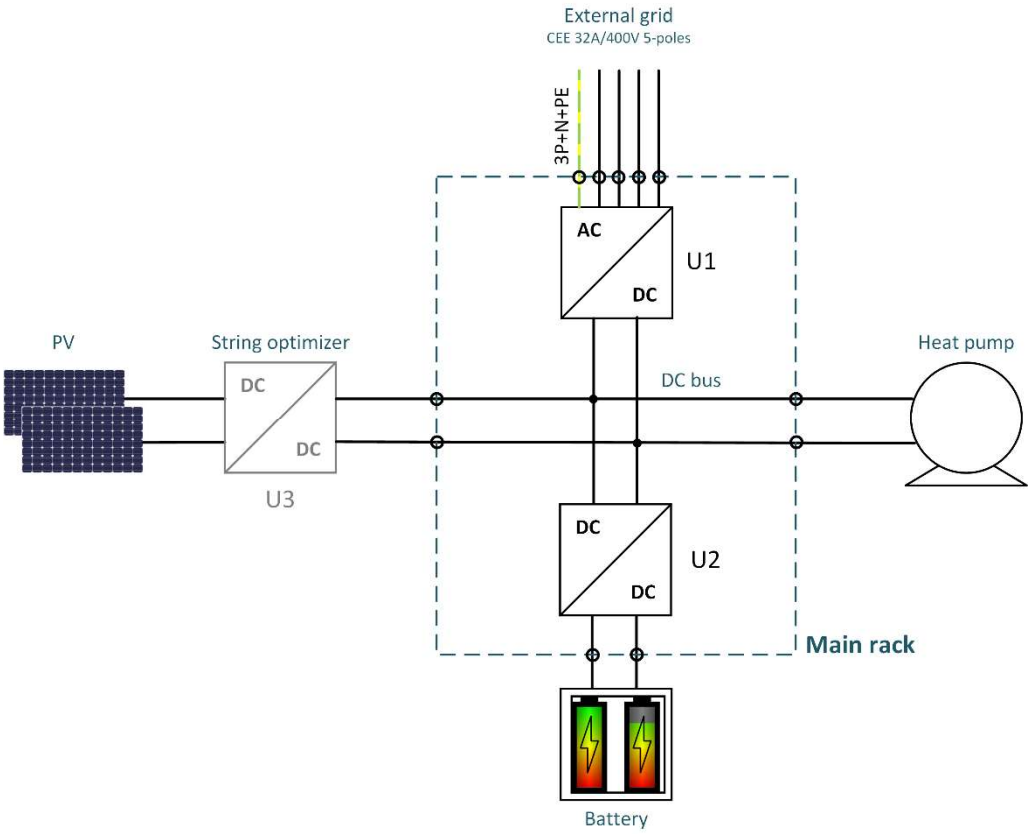


Figure 9: General layout of the DC microgrid and its converters (*U1-U3*)

The developed DC microgrid is meant to interconnect an external AC distribution grid, a DC-supplied heat pump (HP), a battery system and a photovoltaic (PV) installation. This DC microgrid consists of a DC bus and a set of precisely selected converters (*U1* – *U3*). The different components of the system are connected to the DC bus in the following way:

- The 3-phase AC distribution grid is connected to the DC bus by means of the AC/DC converter *U1*.
- The HP is directly connected to the DC bus without converter to avoid conversion losses.
- The battery system is connected to the DC bus by means of the DC/DC converter *U2*. This conversion is mandatory to allow the control of the dis/charge of the battery, to adapt the voltages and guarantee the safety of the battery in case faults.
- The PV installation is connected to the DC bus by means of the DC/DC string optimizer *U3*. This conversion is mandatory for maximum power point tracking (MPPT).

Both *U1* and *U2* are included in the electric demonstrator's main rack, while converter *U3* will be installed close to the PV system on the demo-site. Regarding that last converter, since the

commissioning will be up to the demo-sites, a recommendation on compatible models only will be provided in this document but not a specific device.

Due to the lack of current standardization in the field of low voltage DC (LVDC) regarding voltage levels, the DC bus voltage has been defined based on internal expertise and general availabilities of electric components. The nominal voltage of the DC bus has been defined to 550Vdc.

## 3.2 Definition of constraints for the DC bus converters

Due to the nature of the different system components and the control capabilities needed by the control strategy, a set of constraints limits the number of compatible devices. The main constraints concern the power directionality capability, the voltage compatibility, the power capacity and the control capability. These constraints and their impact on selection process of the converters are presented in Table 1.

Table 1: Description of constraints linked to each converter

| | U1 | U2 | U3 |
|---|---|---|---|
| **Power directionality** | Power may be extracted (local over-consumption) or injected (local over-production) from/to the distribution grid. Thus, the converter needs to be **bidirectional**. | The battery may be charged or discharged. Thus, the converter needs to be **bidirectional**. | The PV installation will only produce power. Thus the converter need to be **unidirectional**. |
| **Voltages compatibility** | On the AC side, the distribution grid is a standard 3-phases connections at **400Vac**. On the DC side, the voltage is set to **550Vdc**. | On the battery side, the battery voltage may fluctuate between **54Vdc to 97.2Vdc**. On the DC bus side, the voltage is set to **550Vdc**. | The voltage on the PV side depends on the size and configuration of the PV installation. On the DC bus side, the voltage is set to **550Vdc**. |
| **Power capacity** | The maximum expected power consumption of the HP is **6kW** (extraction), while the maximum expected PV production is **9kW** (injection). | The maximum continuous current capacity of the battery is 160A, thus a maximum power of **15.5kW**. | The maximum expected PV production is **9kW** (on Almatret demo-site). |
| **Control capability** | The control of the DC side **voltage** is needed to maintain the DC bus voltage. | The control of the battery side **current** is needed to regulate the battery dis/charge. | Embedded MPPT necessary, but no external control capability needed. |

## 3.3 Selection of the most effective DC bus converters

Based on the presented constraints and with the objective of minimizing the bulkiness, the conversion efficiency and the cost, the selected commercially available converters are presented below.

### 3.3.1 U1 – AC/DC grid converter

Two different AC/DC grid converters are being commissioned in the three electric demonstrators. Both converters share the same technical characteristics, but one is cheaper

than the other. Indeed, a new evaluation of available products has been performed after the manufacturing of the first demonstrator due to budget constraints which allowed to find a more profitable solution.

The first selected device is the bidirectional DC power-supply PSB 9750-40 3U (Figure 10) from the German company Elektro-Automatik. This converter equipped the continental electrical demonstrator.

Figure 10: EA bidirectional DC power-supply PSB 9750-40 3U

It has the technical characteristics listed in Table 2 and can be fully controlled and supervised through a CAN bus communication.

Table 2: Main characteristics of the EA bidirectional DC power-supply PSB 9750-40 3U

| Nominal power | DC output voltage | DC output current | Dimension | Weight | Conversion efficiency |
|---|---|---|---|---|---|
| 0 – 10kW | 0 – 750Vdc | 0 – 40A | 449x133x668mm | 25kg | 95% |

Its power capacity allows to fully supply the HP from the grid and offers as well the possibility to fully feed the PV production back to the grid. The DC output voltage range are compatible with the DC bus and its dimensions allows an easy integration into a 19” electric rack.

Although this solution would have been technically suitable for the Mediterranean demonstrators, a more affordable converter has been selected for the latter ones to stay within the budget. This new solution, which is about half the price of the previous one, is the bidirectional DC power supply IT6012C-800-40 (Figure 11) from the Chinese company ITECH.

Figure 11: ITECH bidirectional DC power supply IT6012C-800-40

This converter has similar control capabilities but the communication protocol used is SCPI over TCP/IP. Its technical characteristics are listed in Table 3.

Table 3: Main characteristics of the ITECH bidirectional DC power supply IT6012C-800-40

| Nominal power | DC output voltage | DC output current | Dimension | Weight | Conversion efficiency |
|---|---|---|---|---|---|
| 0 – 12kW | 0 – 800Vdc | 0 – 40A | 449x133x660mm | 34kg | 92% |

Both solutions presented here are laboratory power supplies which offer a lot of functionalities such as battery cycling profiles, solar array emulation, etc. Indeed, these are the most common AC/DC converters which allow a bidirectionality of power. However, only the simple constant voltage output control feature is used in this application. Since all these

offered functionalities have an impact on the product cost, significant savings may be achieved if simpler regenerative DC power supply were commercially available.

### 3.3.2 U2 – DC/DC battery converter

The research of a suitable DC/DC battery converter was the most challenging activity. Indeed, the constraints in terms of controllability and bidirectionality were the major obstacles which arise during the research process. Most of the available devices are either unidirectional (power supply or electronic load) or do not offer a current control capability. Thus, only few suitable devices were available. The cost constraint being taken into account, a single converter remained in the selection, the DC/DC bidirectional converter 80DCDC750DE (Figure 12) from the Finnish company MSc Electronic.

Figure 12: MSc bidirectional DC/DC converter 80DCDC750DE

These converters are manufactured on demands and voltages are adapted by the manufacturer to the client needs. It includes a CANOpen module for control and supervision. The main characteristics of the converter are presented in Table 4.

Table 4: Main characteristics of the MSc bidirectional DC/DC converter 80DCDC750DE

| Battery side voltage | DC bus voltage | Battery side current | Dimension | Weight | Conversion efficiency |
|---|---|---|---|---|---|
| 54 – 97Vdc | 510 – 680Vdc | 0 – 80A | 160x291x512mm | 20kg | 97% |

Although the converter current capacity does not reach the battery current capacity (which is especially high), it will allow a sufficient power flow with the battery comparatively to the HP and PV installation.

This converter implements a single-phase half-bridge conversion structure, composed of two MOSFETs. This simple structure generates a wide range of harmonics which requires to be alleviate by the use of appropriate filters. Moreover, it generates a relatively loud sound in operation. Although suitable for the application, a more advanced (and thus more expensive) converter would ease the implementation and reduce the noise disturbance.

### 3.3.3 U3 – DC/DC string optimizer

As stated above, a specific converter was not selected within the framework of the present report. The purpose of this section is to provide a recommendation of compatible devices to the demo-sites, which will then have the possibility to select the specific model adapted to their PV installation.

The recommended converter are the string optimizers from the US company Ampt, especially series V600 and V750 (Figure 13). This device optimizes the PV production by varying the PV side voltage (MPPT) and automatically adapts to the voltage of the DC bus to which it is connected. The only restriction is that the PV installation has to be splitted into two strings of similar length.

Figure 13: Ampt V600 and V750 string optimizer

The two suggested series cover a wide range of applications, the main characteristic ranges are presented in Table 5.

Table 5: Main characteristics of the Ampt V600 and V750 string optimizer

| MPPT voltage range | DC bus voltage | Output current | Dimension | Weight | Conversion efficiency |
|---|---|---|---|---|---|
| 190 – 700Vdc | 0 – 750Vdc | 0 – 13.5A | ~270x220x100mm | ~4kg | 99.3% |

## 3.4 User interface for control and supervision of the DC bus at demonstrators

In order to allow the manual control and supervision of the DC bus during the testing procedure (and take corrective actions in case of fault of a system component), a dedicated user interface (UI) has been developed. This UI is hosted in the electric demonstrator's PLC and is accessible through a VNC remote access. This UI can thus be accessible by any computer connected to the demonstrator's private network and equipped with a standard VNC client. The complete documentation of the UI will be supplied to the demonstrator at delivery.

The home page of the UI is depicted in Figure 14. The purpose of this page is to provide the operator with a general overview of the state of the system components as well as the measured power flows and voltages. Communication issues or alarms can be easily detected thanks to visual indicators.

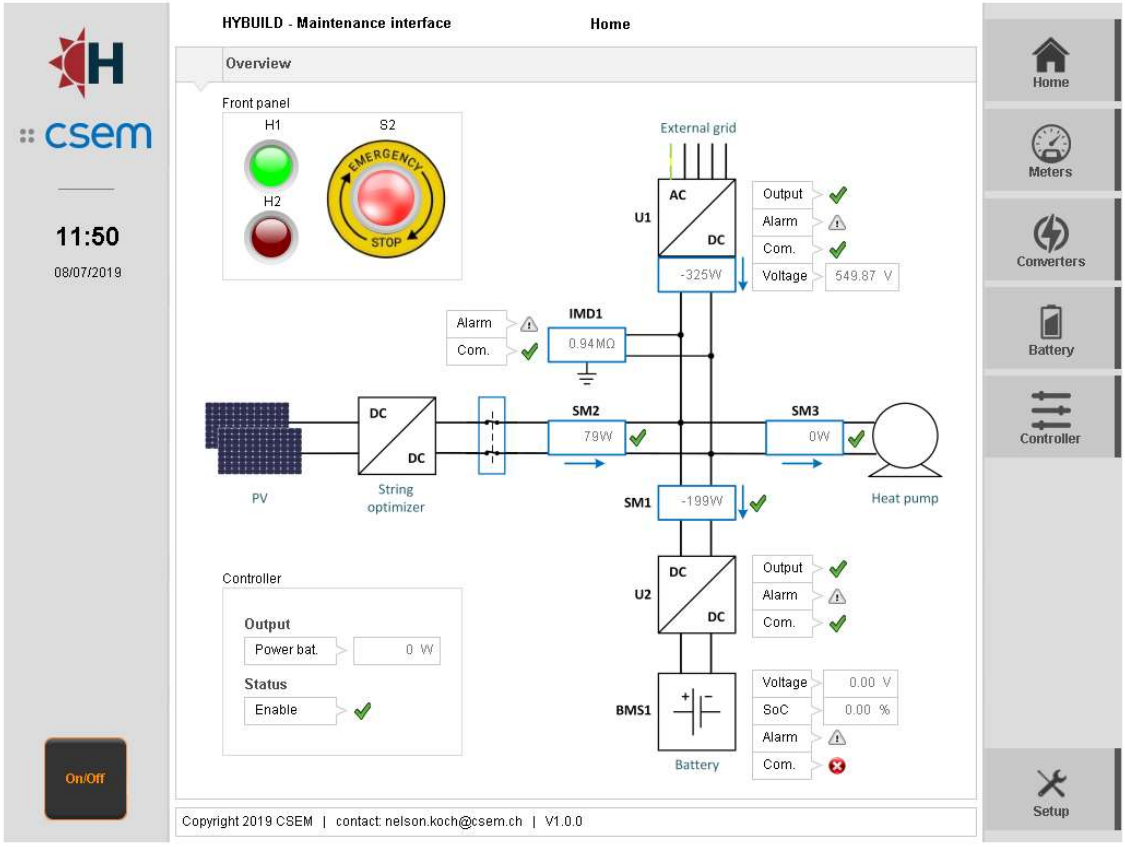


Figure 14: Home page of the UI which provide a general system overview

On the right-hand side, a set of buttons allow to access pages which provide more details for each system components. The pages reached by these buttons are depicted in Figure 15.

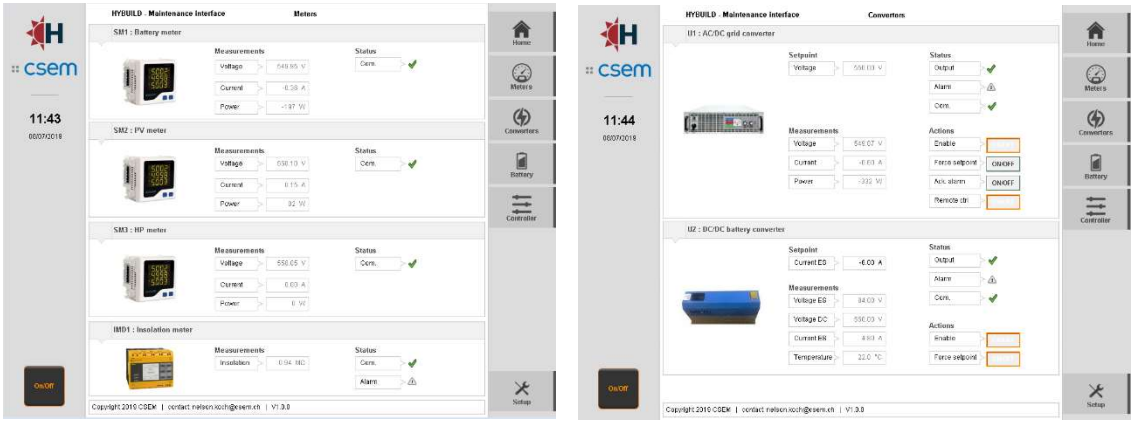

(a) (b)


(c) (d)

**Figure 15: Sub-pages of the UI providing details on: (a) the smart-meters and the irradiation monitor, (b) the converters, (c) the battery and (d) the control strategy**

More in details:

a) The *Meters* page displays the raw data measured by the smart-meters and the irradiation monitoring device. Moreover, the communication status is depicted.
b) The *Converter* page allows not only to read their measurements and status, but also to take manual actions. It is thus possible to manually enable/disable the converters, change their setpoints and acknowledge errors.
c) The *Battery* page provides the complete status of the battery as reported by the BMU. It gathers all its status, warnings and faults as well as the measurements of voltages, temperatures and state of charge. Moreover, this page also allows an operator to manually enable/disable and set/reset the battery in case of fault.
d) The *Controller* page summarizes the status of the control strategy and offers the possibility to manually bypass the master optimizer by manually setting the controller setpoints.

# 4 Integration of heat pump on DC bus and testing

## 4.1 Integration of the heat pump - DC bus

The compression heat pump to be used in the Continental system is equipped with a frequency converter. On the other hand, the Mediterranean heat pump is using a fixed speed compressor, so a separate frequency drive for the compressor has been selected and installed.

On a most simplified level a frequency converter involves two steps: AC/DC conversion and DC/AC conversion. The conversion steps are connected via the DC-link. A control and regulation circuits are used to drive the power electronics in the conversion steps and to control the frequency output of the frequency converter. A simple scheme of a frequency converter is given in Figure 16.

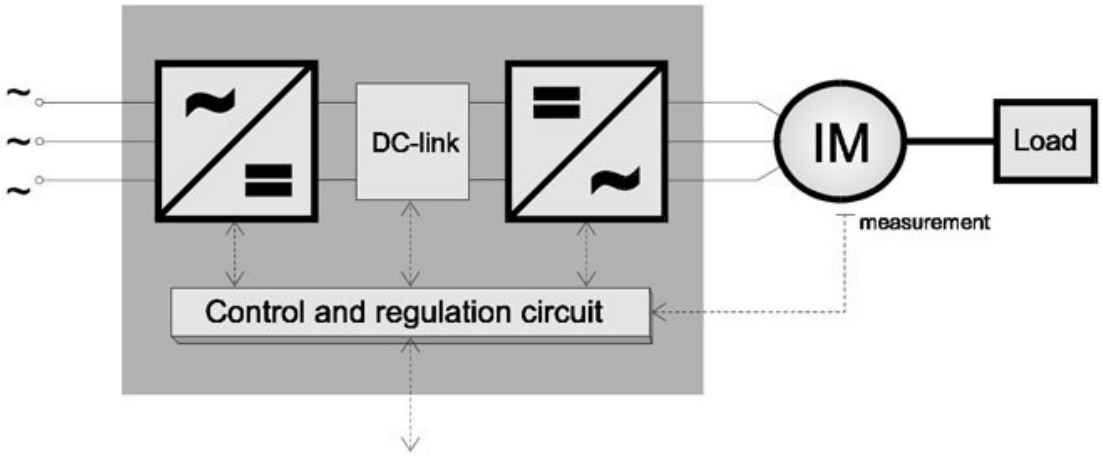


Figure 16 Schematic of a frequency converter.[2]

A frequency converter manufactured by YASKAWA model CIMR-VC4A0011JAB is used in the Continental setup. This frequency converter allows to bypass the first AC/DC conversion step and to directly access the DC-link. The DC bus connection of the frequency converter of the Continental system and the wiring at the AIT lab are illustrated in Figure 17.

[2] http://www.frequencyinverter.org/frequency-converter-basics.html

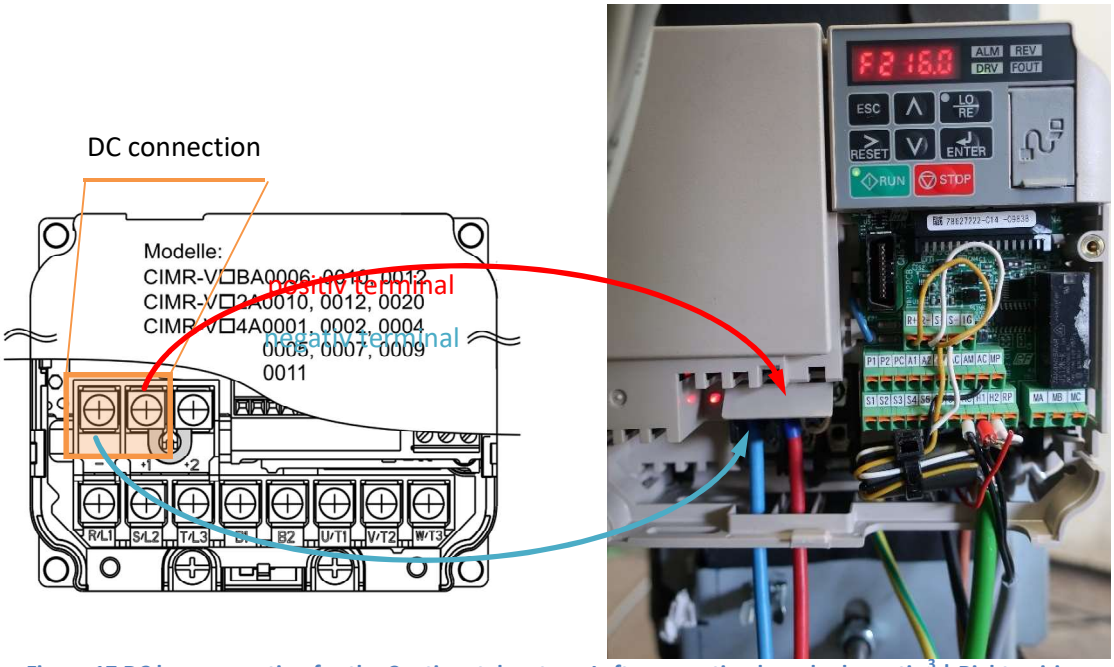


Figure 17 DC bus connection for the Continental system. Left: connection board schematic [3] | Right: wiring.

For DC-bus testing the compression heat pump was connected to a controlled DC generator which allows to adjust the DC supply to the frequency converter accordingly. The DC generator and the software interface are illustrated in Figure 18.


Figure 18 DC bus generator (left) and software interface (right).

For the Mediterranean system, a DC powered, air cooled drive (being actually an Inverter unit) was especially selected for the HYBUILD application. This unit is manufactured by VACON (INU series, model NXI0095) and its supply voltage varies in the range of 380 – 500VDC.

In order to simulate the DC grid during the lab testing of the heat pump, an Active Front End AC/DC converter from Vacon (model AFE NXI00125), is used.

[3] YASKAWA, 2011. *YASKAWA Frequenzumrichter V1000 - Kompakter Frequenzumrichter mit Vektorregelung - Technisches Handbuch*. YASKAWA HANDBUCH NR. SIGP C710606 19A.

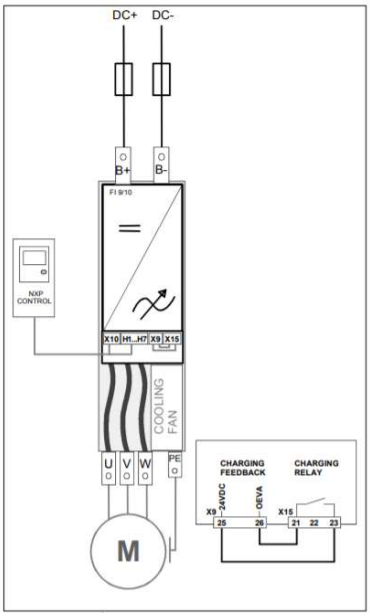


Figure 19: Wiring diagram of the Vacon NXI inverter unit installed on the Daikin heat pump

## Continental heat pump - DC bus hardware-in-the-loop-testing

### 4.1.1 Measurement setup

The measurement setup involves the sensors and data acquisition system described in "Deliverable 3.2 – Configuration of the hard- and software interfaces of the DCS finished". In addition, the system was equipped with an electric power meter, Nemo D4-DC from Legrand, which allows to measure electric current, voltage and power simultaneously with an accuracy of at least ±1%.

### 4.1.2 Test cases

The DC bus connection of the heat pump is tested against the operation limits given by the frequency converter manufacturer which accepts DC supply voltages between 510…680VDC. The selected and measured DC supply voltages are listed in Table 6.

Table 6 DC supply voltage test conditions.

| ITEM | UNIT | VALUE AND VARIANCE |
|---|---|---|
| DC-1 | VDC | 510 |
| DC-2 | VDC | 680 |
| DC-3 | VDC | 595 |

### 4.1.3 Heat pump operating conditions

The heat pump setup is operated at stable conditions to avoid falsification of the results. Key measured operating parameters of the heat pump are given in Table 7.

Table 7 Key heat pump operating parameters

| ITEM | UNIT | VALUE AND VARIANCE |
|---|---|---|
| Ambient | | |
| temperature | °C | 2.41 ± 0.26 |
| rel. humidity | % | 75.13 ± 0.45 |
| Water | | |
| return temperature | °C | 31.16 ± 0.15 |
| feed temperature | °C | 38.25 ± 0.13 |
| mass flow | kg/s | 0.25 ± 0.00 |
| Heat pump | | |
| compressor rotations | % | 60 |

### 4.1.4 Results

The effect of different DC supply voltages has been analysed for 15 minutes for each test case and time dependent results are given in Figure 20. Switching between the test cases was smooth and caused no interruption of operation. While the DC supply voltage had little effect on the compression ratio an effect on the electric power $P_{el}$ is obvious. The increase of supply voltage from case DC-1 to DC-3 caused an increased electric consumption of about 0.93% while between DC-1 and DC-2 an increase of 1.53% has been observed. Further, a minor fluctuation of the thermal power $P_{th}$[4] has been observed which is most likely caused by the inherent dynamics in heat pump operation with the RPW-HEX in the refrigerant cycle. Results from the testing of the DC bus are given in

Table 8 in tabular form.

Table 8 Results from DC-bus testing including standard deviation of measurement values.

| Test case | Voltage in V | Current in A | CPR | $P_{el}$ in W | $P_{th}$ in W |
|---|---|---|---|---|---|
| DC-1 | 515.8 ± 0.09 | 3.8 ± 0.01 | 3.7 ± 0.01 | 1969.8 ± 5.64 | 7242.9 ± 94.05 |
| DC-2 | 687.6 ± 0.12 | 2.9 ± 0.00 | 3.7 ± 0.01 | 1999.8 ± 2.72 | 7311.6 ± 56.43 |
| DC-3 | 601.7 ± 0.06 | 3.3 ± 0.01 | 3.7 ± 0.01 | 1988.1 ± 4.18 | 7389.4 ± 68.53 |

### 4.1.5 Conclusions

DC bus operation of the heat pump system has been successfully accomplished. The frequency converter has been tested in the manufacturer given DC supply range between 510…680VDC. While the system had no difficulty to adapt to the new DC supply an overall increase of electricity consumption with supply voltage is indicated.

[4] The thermal power is calculated from mass flow and temperature measurements.

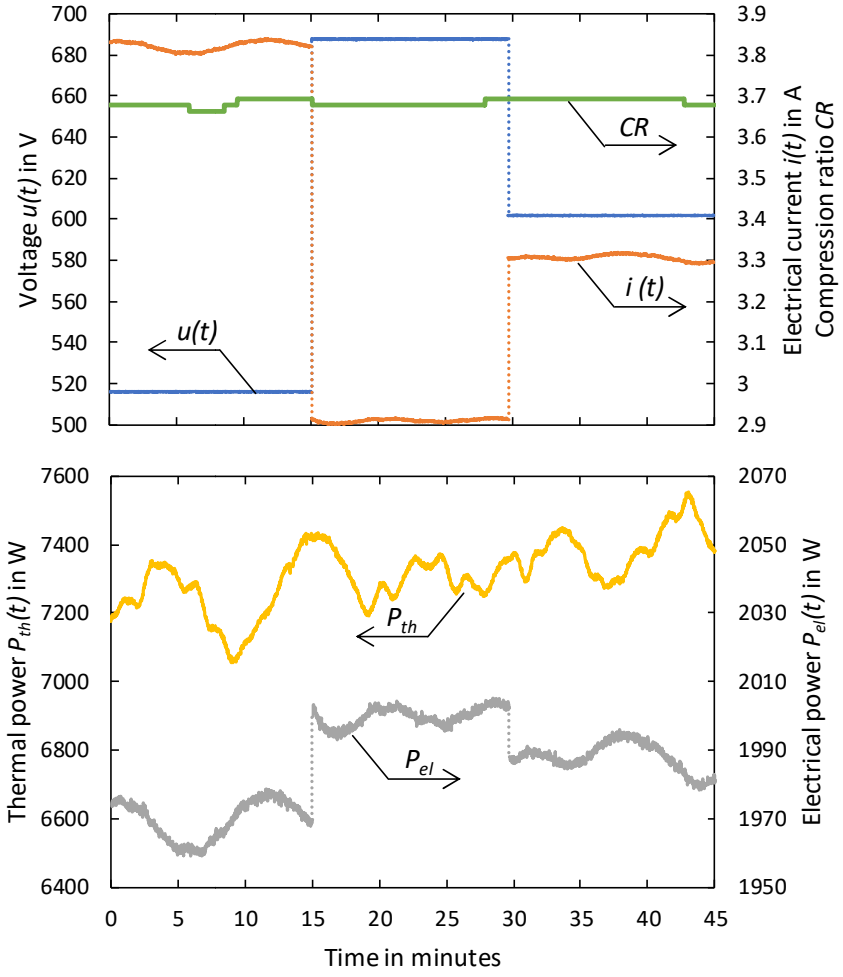


**Figure 20 Result from DC bus testing. Top: Measured DC voltage *u(t)* and current *i(t)* as well as compression ratio *CR*. Bottom: Measured thermal power $P_{th}$ and electrical power $P_{el}$.**

## 4.2 Mediterranean heat pump – Electrical tests on the compressor

As for the Mediterranean heat pump, since the customization of the heat pump in order to support a DC driven frequency converter is still on-going, selected results from the preliminary tests if the heat pump before and after interventions, needed for the sizing and selection of the motor drive are presented.

The pre-intervention tests were conducted under the conditions specified in the table below:

Table 9 Pre intervention testing conditions for the Mediterranean heat pump

| ITEM | UNIT | VALUE AND VARIANCE |
|---|---|---|
| Test duration | min | 130 |
| Evaporator water inlet temperature | °C | 10 ± 1 |
| ΔT in evaporator | °C | 5 ± 0.5 |
| ΔT in condenser | °C | 5 ± 0.5 |
| Supply Voltage of the compressor | V | 405 ± 5V |
| Compressor frequency | Hz | 50 |

The outlet temperature of the water was left as a parameter, under the assumption that for a fixed evaporator temperature conditions, increased temperatures in the condenser should lead in higher power consumptions. Given that the heat pump in cooling mode will mainly operate in low condensation temperatures, due to the cascaded Compression heat Pump – Sorption Chiller concept, the highest condenser temperatures are expected during the heating period. As a result, tests were focused on water outlet temperatures in the condenser up to 45°C. Besides, the electrical parameters of the compressor during the start-up were recorded, in order to identify possible overshoots of the line current. The results obtained are shown in Figure 21.

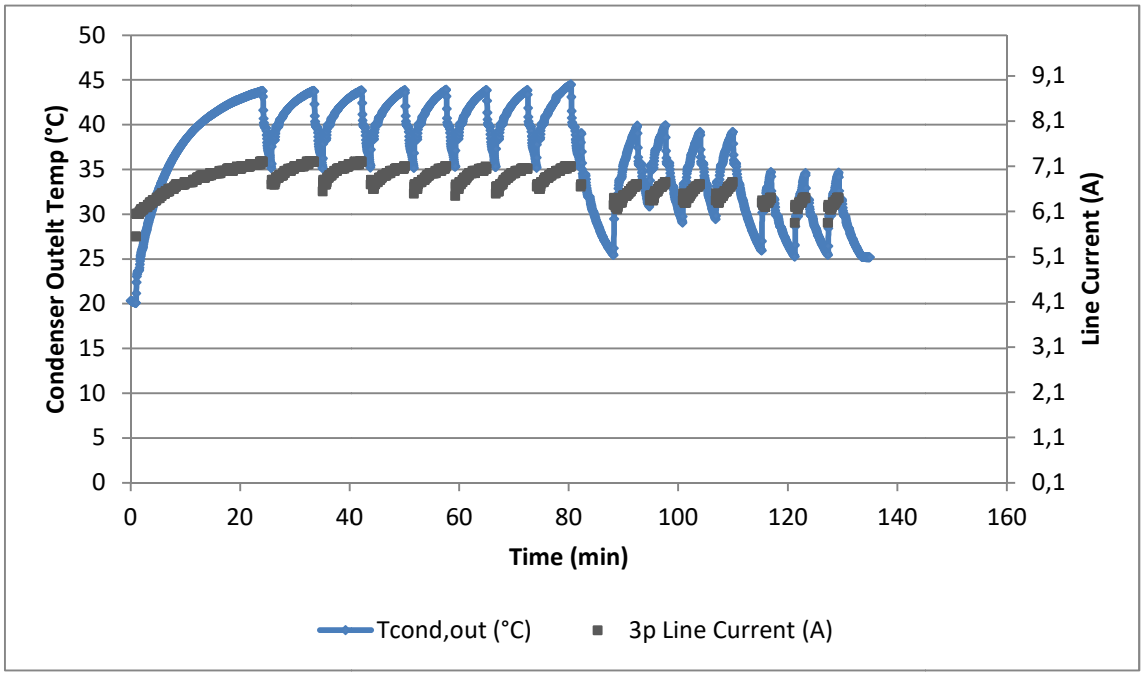


Figure 21 3p Line Current and condenser outlet water temperature in pre-intervention tests of the Mediterranean heat pump

It can be easily determined that the line current does not exceed the value of 7.15 A, which corresponds to a set-point of 45 °C of the water and goes down to 6.20 A for a condenser outlet water temperature around 35°C, which correspond to the rated conditions of the heat pump. During the many on-off cycles no overshoots were identified in the current response. Given these conditions, the Vacon Inverter Unit mentioned in Section 4.1was selected.

During the same test, the value of the PF is also presented, being also an important parameter for the selection of the frequency drive (Figure 22).

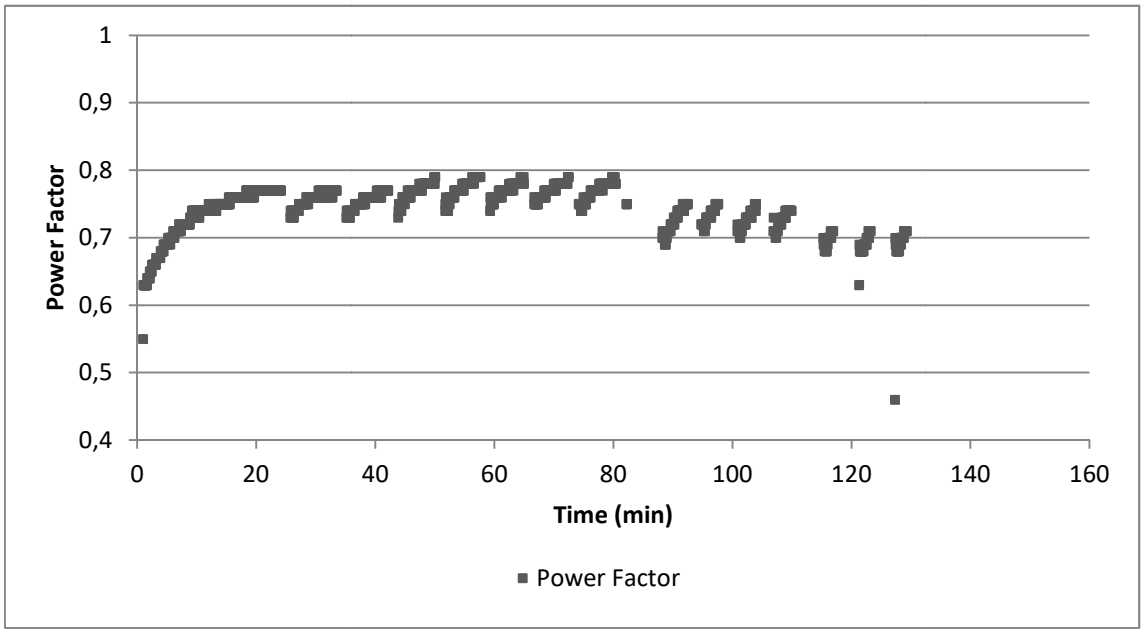


Figure 22 Mediterranean heat pump Power Factor under the pre-intervention testing

As for the post interventions tests, the electrical parameters were checked in almost rated temperature conditions on both the evaporator and condenser hydraulic circuits, which are summarized in the following table:

Table 10 Post intervention testing conditions for the Mediterranean heat pump

| ITEM | UNIT | VALUE AND VARIANCE |
|---|---|---|
| Test duration | min | 80 (at t=25 min, the heat pump is switched off and the refrigerant and water flows are diverted to the RPW-HEX) |
| Evaporator water inlet temperature | °C | 15 ± 1 |
| ΔT in evaporator | °C | 4 ± 0.5 |
| Condenser water inlet temperature | °C | 35±1 |
| ΔT in condenser | °C | 4 ± 0.5 |
| Supply Voltage of the compressor | V | 405 ± 5V |
| Compressor frequency | Hz | 50 |

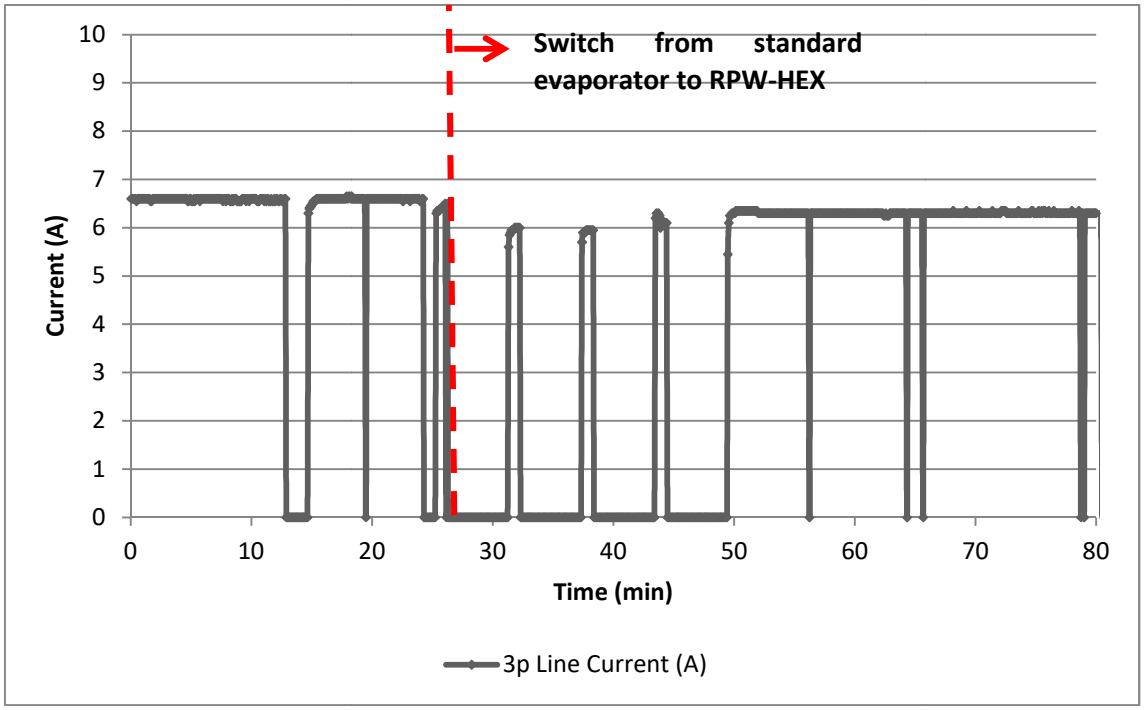


Figure 23 3p line current of the Mediterranean heat pump compressor in post intervention tests for operation with the standard and the RPW heat exchanger

It is clear that after the interventions on the refrigerant circuit of the heat pump and the installation of the RPW-HEX, no important differences are noted, apart from a relatively increased current on the compressor during standard evaporator operation compared to the expected values from the pre-intervention tests (an increase of about 0.4 A). This can be attributed to either an overcharged system (due to the discrepancies between the RPW-HEX and standard evaporator volumes) or the increased pressure drops on the solenoids and the additional piping. On the other hand, the current of the compressor seems to decrease when the heat pump operates with the RPW-HEX. This can be explained considering the lower pressure drop of the RPW-HEX compared to the respected value of the standard evaporator. All in all, the value of the 3-phase line current drawn by the compressor in the original and the retrofitted system can be assumed to be almost unaffected.

# 5 Advanced process monitoring of heat pumps operation

The key performance indicator for heat pumps current operating state is the coefficient of performance (*COP*) which compares the useful heat $P_{th}$ to the work *W* required.

$$COP = \frac{P_{th}}{W}$$

In case of cooling, the performance indicator is defined analogously to the COP but is referred as Energy Efficiency Ratio (EER), defined as:

$$EER = \frac{P_{th}}{W}$$

where $P_{th}$ corresponds to the absorbed heat from the cooled medium(usually water or air).

For an electric driven heat pump the work *W* corresponds to the electricity demand $P_{el}$. To capture the efficiency of the heat pump system for different operating conditions occurring

over the year the seasonal performance factor (*SPF*) is used which compares the produced energy to consumed energy.

$$SPF = \frac{\int P_{th}\, dt}{\int P_{el}\, dt}$$

To capture the average performance over a shorter period the performance factor may also be calculated on a shorter time basis including months, days or hours. This will correspond to a monthly, daily or hourly performance factor.

However, determining these key indicators requires knowledge of $P_{th}$ and $W$ or $P_{el}$ respectively. While $W$ or $P_{el}$ typically are a result of direct measurement $P_{th}$ must be derived indirectly from determination of enthalpies and mass flow. Due to the heat pump system inherent phase change of the refrigerant both are challenging to access. For systems with thermal storages the inherent dynamics further increases complexity.

In the later heat pump performance monitoring approaches for the Continental and Mediterranean system are discussed.

### 5.1.1 Monitoring of the Continental system

For the Continental system the useful heat $P_{th}$ exerts two components: the heat transferred via the condenser $\dot{Q}_{cond}$ and the useful heat from the RPW-HEX $\dot{Q}_{RPW}$. It is important to mention that useful heat from the condenser in the Continental setup can be heat or cold depending on the operating mode. The heat or cold from the condenser can be derived from the water-side or from the refrigerant side either. However, due to unclear state of the refrigerant at the condenser outlet – it can be two-phase or liquid – the transferred heat must be derived from the water side by

$$\dot{Q}_{cond} = \dot{m}_{cond} \cdot (h(p,\vartheta)|_{outlet} - h(p,\vartheta)|_{inlet})|_{cond,water}$$

Here $\dot{m}_{cond}$ reflects the mass flow of water and $h$ the enthalpy of the water at the condenser inlet or outlet respectively. For the RPW-HEX $\dot{Q}_{RPW}$ may be determined from the water $\dot{Q}_{RPW,water}$ or refrigerant $\dot{Q}_{RPW,refrigerant}$ side with the limitation to discharging operation for the water side approach. However, the energies must correspond over time if the time interval is sufficiently long

$$E_{RPW} = \int \dot{Q}_{RPW,water} dt = \int \dot{Q}_{RPW,refrigerant} dt$$

where

$$\dot{Q}_{RPW,water} = \dot{m}_{RPW} \cdot (h(p,\vartheta)|_{outlet} - h(p,\vartheta)|_{inlet})|_{RPW,\boldsymbol{water}}$$

$$\dot{Q}_{RPW,refrigerant} = \dot{m}_{RPW} \cdot (h(p,\vartheta)|_{outlet} - h(p,\vartheta)|_{inlet})|_{RPW,\boldsymbol{refrigerant}}$$

It is important to note that in a real system the energy balance must account for the energy losses as well.

With this the COP for the Continental system is

$$COP = \frac{\dot{Q}_{cond} + \dot{Q}_{RPW,water}}{P_{el}}$$

where $\dot{Q}_{RPW}$ is determined from the water side to cover the dynamics of the thermal storage.

The performance factor is

$$PF = \frac{\int \dot{Q}_{cond}\, dt + \int \dot{Q}_{RPW}\, dt}{\int P_{el}\, dt} = \frac{\int \dot{Q}_{HP}\, dt}{\int P_{el}\, dt}$$

where

$$\int \dot{Q}_{RPW}\, dt = \int \dot{Q}_{RPW,refrigerant}\, dt - E_{loss} = \int \dot{Q}_{RPW,water}\, dt$$

and $\dot{Q}_{HP}$ is the heat transferred by the heat pump taking inlet and outlet water temperature in account.

The measurements needed to determine the values needed for the determination of useful heat are given in Table 11 and the position of the measurements are given in Figure 24.

**Table 11 Heats and measurement points**

| Item | Measurements |
|---|---|
| $\dot{Q}_{cond}$ | FTI-21, TI-22, TI-23, PI-28 |
| $\dot{Q}_{RPW,water}$ | FTI-21, FTI-25, TI-34, TI-26, PI-28 |
| $\dot{Q}_{RPW,refrigerant}$ | FTI-8, TI-4, PT-3, TI-6, PDTI-5 |
| $\dot{Q}_{HP}$ | FTI-21, TI-17, TI-37, PI-28 |

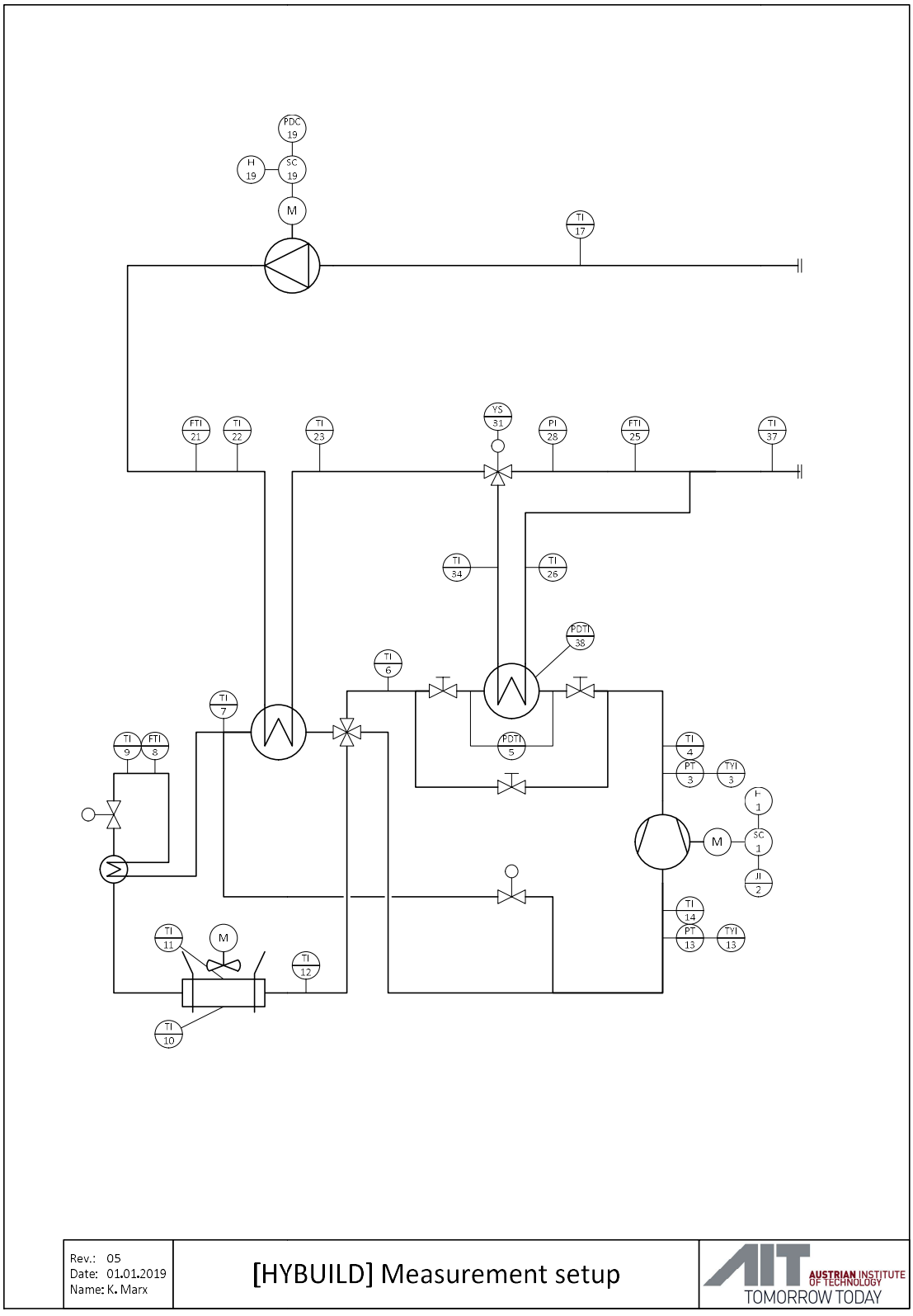


Figure 24 Measurement setup.

#### 5.1.1.1 Results

To test the advanced monitoring algorithms the Continental heat pump system was operated in continuous RPW-HEX charging/discharging operation for several hours. Temperatures,

pressures and flows were continuously monitored and stored at high frequency[5]. Figure 25 shows operation of the heat pump in charging and discharging operation for more than 50 hours covering 7 RPW-HEX charging and discharging cycles.

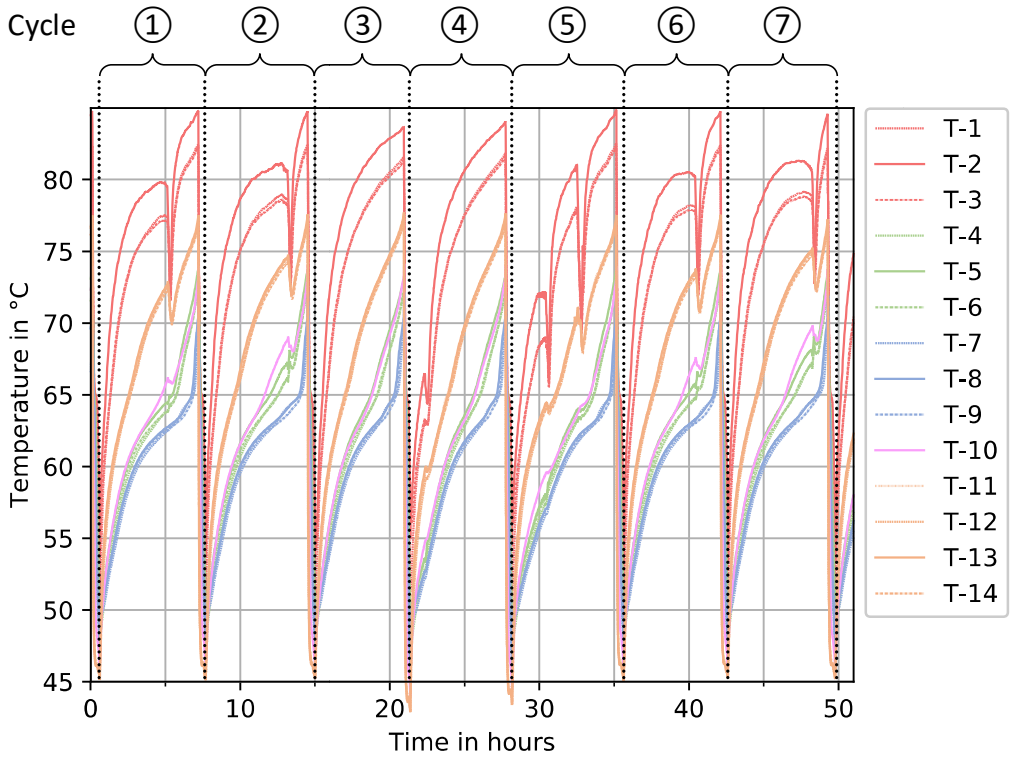


**Figure 25 Operating experience of the Continental heat pump system for more than 50 hours covering 7 RPW-HEX charging and discharging cycles. The graph shows surface temperatures of the RPW-HEX.**

Based on online measurements the heat transferred from the refrigerant to the PCM inside the RPW-HEX ($\dot{Q}_{RPW,refrigerant}$) based on measurements in the refrigerant cycle, the heat transferred from PCM inside the RPW-HEX to the water ($\dot{Q}_{RPW,water}$) based on measurements in the water, the heat transferred from refrigerant to water inside the condenser ($\dot{Q}_{cond}$) based on measurements in the water as well as heat transferred from the heat pump to the water ($\dot{Q}_{HP}$) based on measurements in the water at the inlet and outlet of the heat pump was derived. The transferred heats for the charging and discharging cycle ① from Figure 25 are shown in Figure 26. Charging requires about 6.5h where in parallel about 5-9 kW (depending on the thickness of the ice on the evaporator) of heat are delivered to the heating system at approx. 43°C. After about 4.5h a defrosting cycle is started for ice removal from the evaporator of the heat pump. This results in a negative heat flow since thermal energy must be delivered to the condenser to cover the evaporation inside the condenser in reverse/defrosting operation. After about 6.6 hours RPW-HEX charging the discharging process is started resulting in a steep increase of heat flow reaching a maximum at about 32 kW.

[5] For more details see Deliverable „D3.2 - Configuration of the hard- and software interfaces of the DCS finished"

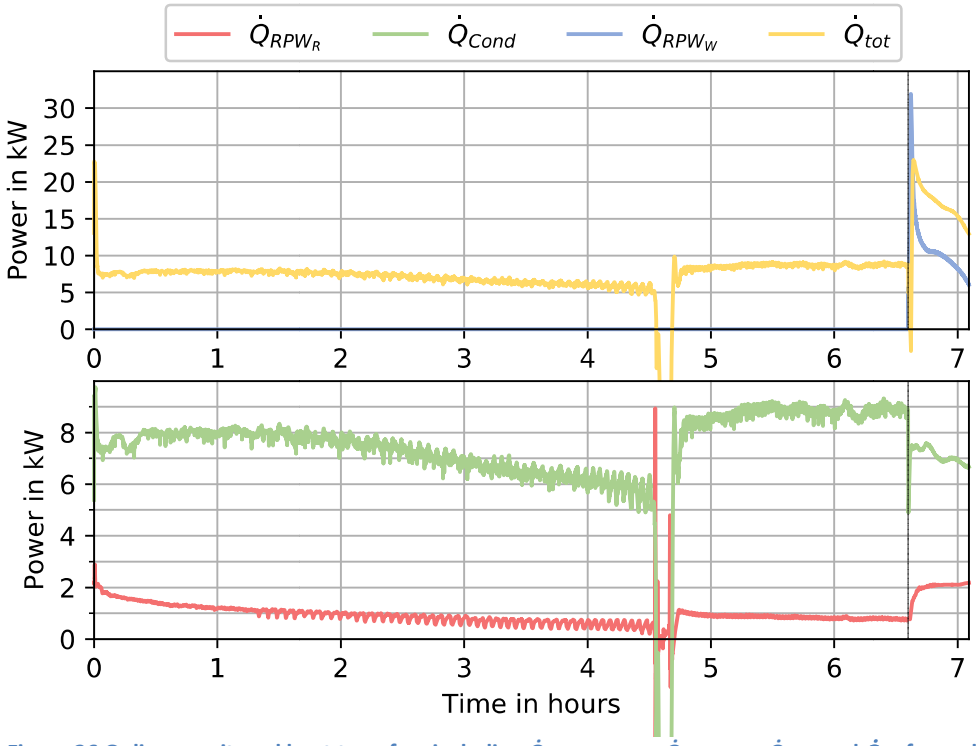


Figure 26 Online monitored heat transfers including $\dot{Q}_{RPW,refrigerant}$, $\dot{Q}_{RPW,water}$, $\dot{Q}_{cond}$ and $\dot{Q}_{HP}$ for cycle ②.

Accumulated thermal $E_{th}$ and electric $E_{el}$ energy from the cycle given in Figure 26 as well as COP and the cycle related performance factor *CPF* is given in Figure 27. For heating operation, the COP ranges between 2-2.8. At the beginning of the discharging the COP shows a sharp increase due to the significant heat release from the RPW-HEX. The CPF reflecting the performance of the heat pump for the entire cycle is 2.55 which includes heating and DHW generation.

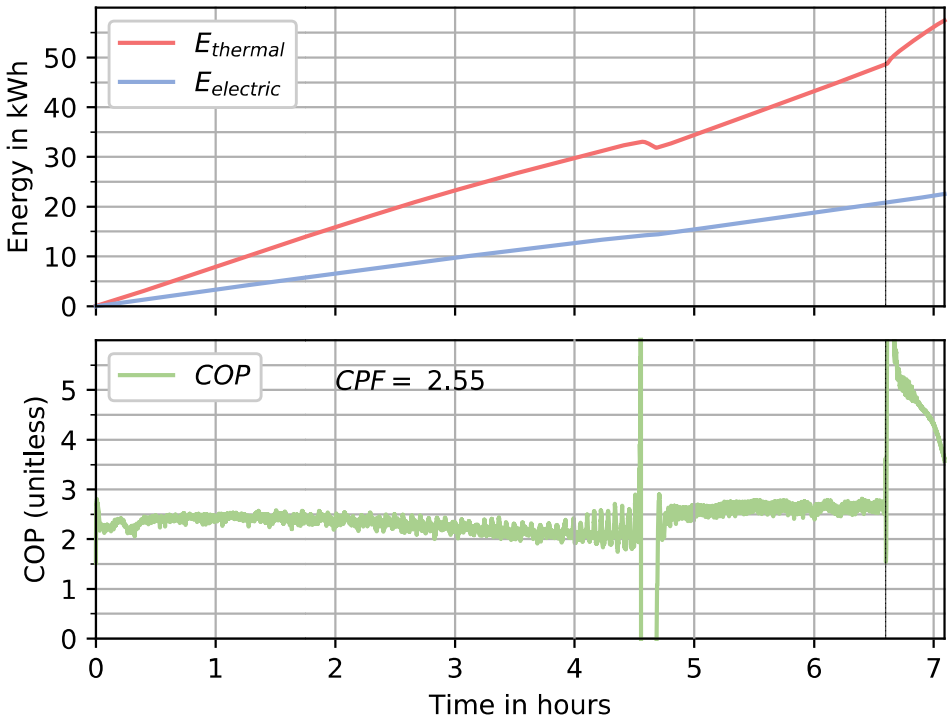


Figure 27 Accumulated thermal $E_{th}$ and electric $E_{el}$ energy as well as COP and CPF for cycle ②.

### 5.1.2 Monitoring of the Mediterranean system

For the Mediterranean system the useful thermal energy is the one obtained from the evaporator of the heat pump. Even though this value is easy to be determined with measurements on the water side for the standard evaporator, the case for the RPW-HEX is much more complicated. When the RPW-HEX is in operation, the heat balance among the three streams is:

$$\dot{Q}_{PCM} + \dot{Q}_W = \dot{Q}_r - \dot{Q}_{loss}$$

Where the subscripts PCM, W, r and loss correspond to the net heat flow to or from the PCM, water, refrigerant the heat losses respectively.

As a result, the momentary EER of the heat pump may be written as follows:

$$EER = \frac{\dot{Q}_r - \dot{Q}_{loss}}{P_{el}} \cong \frac{\dot{Q}_r}{P_{el}}$$

assuming that the instantaneous value of the heat losses is relatively small compared to the other variables.

Apart from the electrical consumption of the compressor, which can be directly monitored from a power meter or the frequency drive, the definition above implies that the inlet and outlet enthalpies of the evaporator and the refrigerant mass flow rate should be known. Given that the pressure and the temperature at the outlet of both the evaporator and the condenser are measured and the enthalpy at the outlet of the receiver can be assumed to be equal to the bubble enthalpy of the refrigerant for the measured condensation pressure and almost equal to the enthalpy at the inlet of the evaporator, the only unknown parameter is the refrigerant mass flow rate. This value can be estimated as follows:

Calculate the $\dot{Q}_{cond}$ heat flow as a function of the measured water temperatures and flow rate on the water side of the condenser:

$$\dot{Q}_{cond} = \dot{m}_w c_{pw}\left(T_{w_{cond,out}} - T_{w_{cond,in}}\right)$$

Then, using the measured condenser pressure and inlet temperature values and assuming negligible losses on the condenser, the refrigerant mass flow rate can be estimated from the following expression:

$$\dot{m}_{ref} = \frac{\dot{Q}_{cond}}{h\left(p_{cond}, T_{cond,in}\right) - h\left(p_{cond}, T_{cond,out}\right)}$$

Since the outlet pressure of the condenser is almost equal to the receiver pressure, the outlet enthalpy of the receiver can also be evaluated:

$$h_{liqreceiv,out} = h_l(p_{cond})$$

And assuming an isenthalpic expansion in the expansion valve it is

$$h_{evap,in} = h_{liqreceiv,out}$$

As previously mentioned, the pressure and temperature at the outlet of the evaporator is measured, thus:

$$h_{evap,out} = h\left(p_{evap,out}, T_{evap,out}\right)$$

So:

$$\dot{Q}_r = \dot{m}_{ref}\left(h_{evap,out} - h_{evap,in}\right)$$

This procedure allows the determination of the $Q_r$ value based on real time measurements but imposes errors due to the required assumptions and the variety of the utilized sensors, with each of them adding uncertainty to the calculations. Besides, the aggregated error due to the neglected heat losses from the RPW-HEX can be relatively decisive when the system's performance over a testing period is assessed.

As a result, it is more convenient to assess a seasonal performance factor on a daily basis, especially since the latent storage charge/discharge time scale is significantly lower. So, on a daily basis one can assume that:

$$\int \dot{Q}_{PCM} dt \cong 0$$

And

$$\int \dot{Q}_W dt \cong \int (\dot{Q}_r - \dot{Q}_{loss}) dt$$

So

$$SPF = \frac{\int \dot{Q}_W dt}{\int P_{el} dt}$$

Where $Q_w$ is calculated using the measured water temperatures and volumetric flow.

#### 5.1.2.1 Results

The next figure validates the calculation procedure described in the section above over a 7 min operation cycle of the Mediterranean heat pump. The installed sensors used to calculate the required parameters in order to complete the calculation procedure described in the previous section are included in Figure 3 and Figure 4. During the test, the condenser conditions were kept almost constant with a condensing temperature equal to 33.5 ± 0.5 °C and a ΔT equal to 5°C. The instantaneous EER value is plotted against the inlet evaporator temperature and the evaporator cooling capacity (in kW), showing an expected decrease of the EER from the value of 3.2 to a value of 2.5 when the evaporator inlet temperature is decreasing from 16°C to almost 10 °C. Besides, the cooling capacity of the heat pump is also decreased.

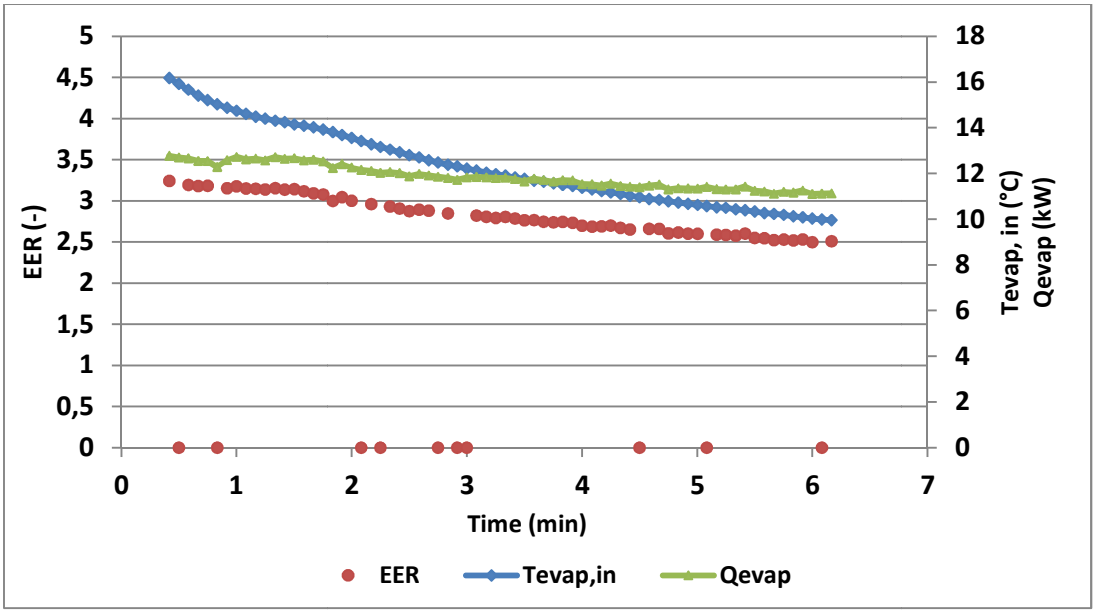


Figure 28 Monitored EER and evaporator capacity values for varying evaporator inlet temperature of the Mediterranean heat pump

The following figure depicts the calculated refrigerant mass flow rate through the experiment, along with the pressure ratio (equal to $p_{cond}/p_{evap}$) of the compressor. A small decrease on the mass flow rate can be noticed, which can be attributed to increased compressor leakages and lower evaporation pressure (which causes the TEXV to close a bit as well).

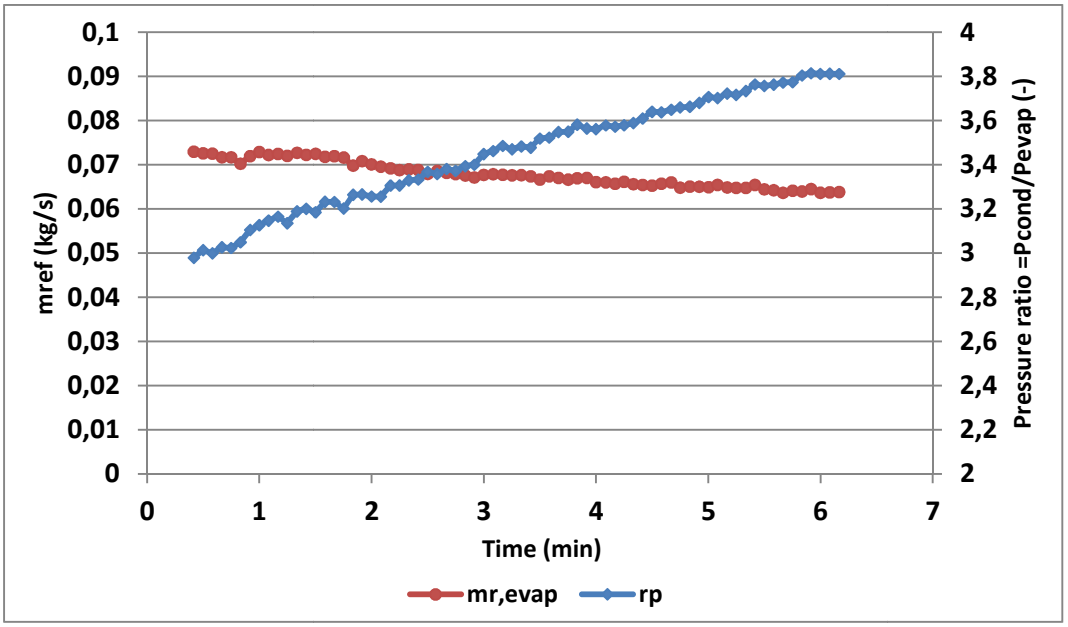


Figure 29 Monitored refrigerant mass flow rate versus the compressor pressure ratio of the Mediterranean heat pump

# 6 Conclusions

Both the Continental and the Mediterranean heat pumps were modified for direct connection to a DC grid. The required frequency drives were identified and properly sized in order to be compatible with the developed DC grid design and equipment. Operational tests on the Continental heat pump validated the technology. On the other hand, AC electrical tests on the Mediterranean heat pump before and after the installation of the RPW-HEX defined the boundary conditions needed in order to select and acquire a frequency converter in order to allow the DC connection of the heat pump on the demo site's DC grid.

Besides, monitoring protocols for the instantaneous and seasonal performance indicators of both the heat pumps, based on real time data available from the installed sensors, were defined. Even though measuring the instantaneous COP and EER values for the Continental and the Mediterranean heat pumps respectively can be achieved through assumptions (and provided that the state of the refrigerant at the outlet of the condenser not in the two-phase region for the continental design), using a Seasonal Performance Factor based on the measured values on the water side for both the system can directly lead to more reliable results, provided that this Factor refers to a long enough time period. Example of the monitoring for both cases in lab environment was given, proving the feasibility of the algorithms.